IEEE Access
Multidisciplinary | Rapid Review | Open Access Journal

Received June 16, 2019, accepted June 26, 2019, date of publication July 3, 2019, date of current version July 23, 2019.

Digital Object Identifier 10.1109/ACCESS.2019.2926538

Detection and Location of Stator Winding Interturn Fault at Different Slots of DFIG

SHUILONG HE, XUHONG SHEN, AND ZHANSI JIANG
School of Mechanical and Electrical Engineering, Guilin University of Electronic Technology, Guilin 541004, China

Corresponding author: Shuilong He (xiaofeilonghe@163.com)

This work was supported in part by the Project of National Natural Science Foundation of China under Grant 51565008, in part by the Innovation-Driven Development Special Fund Project of Guangxi under Grant Guike AA18242033 and Grant Guike AA18242036, in part by the GUET Excellent Graduate Thesis under Grant 17YJPYSS02, and in part by the Innovation Project of Guet Graduate Education under Grant 2019YCXS001.

ABSTRACT Generators are critical components for the wind power generation system and process industries. Generating units or production lines may be shut down by generator failure. Most of the methods used in previous research have analyzed the rotor winding interturn fault in the slot location or the stator winding interturn fault in the phase location, but the doubly fed induction generator (DFIG) stator fault in the slot location still needs to be studied further because of the special topological structure and the real factors of the generator model. To solve this problem, this paper determines the pulsating magnetomotive force (MMF) expressions mapped to the shorted position in two forms. Based on 2D discretization and piecewise interpolation, by taking the short-circuit number and the position of short-circuit slot as model parameters, the modified fault model is developed. The simulations show that as an interturn short-circuit fault occurs, the stator's three-phase current is no longer symmetric, where the fault-phase current is bigger than that in healthy operation. In addition, the results show that the interturn short-circuit faults induce negative sequence current that increases with the gravity of fault in the DFIG stator and that the phase difference of the fault-phase and its lagging phase is more than 120°. Moreover, commonality and heterogeneity existing in the current amplitude and negative sequence features for detecting stator interturn faults at different slots of the DFIG are proposed and analyzed. The results obtained in this paper are important complements to the stator interturn short-circuit analysis and help the practical monitoring and diagnosis of this fault.

INDEX TERMS DFIG, stator winding interturn short circuit, short-circuit slot, negative sequence, heterogeneity.

I. INTRODUCTION

With the rapid development of wind power technology, China's wind power industry has dramatically increased. Doubly-fed wind turbines are used more and more widely, with growing capacity. Because the doubly-fed induction generator (DFIG) working environment is poor, its smooth operation is affected. The occurrence of generator faults is a major factor affecting smooth operation, including mechanical failure and electrical failure. Induction-machine stator winding insulation degradation is one of the major causes (about 40%) of machine failure [1], [2]. The stator winding interturn short circuit is a typical electrical fault, and the stator faults begin with the degradation of the insulation between turns, and consequently, an interturn short circuit occurs [3]. Then, the phase-ground or phase-to-phase short circuit occurs, as verified by the stator winding short-circuit fault of a permanent magnet synchronous machine [4].

Existing studies on models, simulations, and experiments of DFIG's stator winding interturn faults are well documented [5]–[9]. There are two main methods for the modeling of the interturn short circuit of the stator windings of the DFIG. One method uses the multi-loop theory to build the mathematical model in ABC three-phase static coordinate system [10] and deduce the mathematical model in the dq0 synchronous rotating coordinate system [11]. Another method is based on the finite element theory, where a 2D electromagnetic field model is established in the finite element software ANSYS Maxwell. Models presented in studies for a winding interturn short-circuit fault are achieved by changing the number of shorted turns and value of short-circuit resistance according to the ratio of the normal turns to short turns [12], [13], [14].

Recently, electrical parameters such as current and voltage have attracted the most attention in research, where current

The associate editor coordinating the review of this manuscript and approving it for publication was Yanzheng Zhu.

is the most widely used. Features extracted from the current signal are used for fault detection and are obtained using several signal processing methods such as time-domain analysis, frequency-domain analysis, and time-frequency-domain analysis [15]. Reference [16] analyzed the negative sequence current of the rotor three-phase current and took it as the characteristic of the fault. The negative sequence impedance method was used to distinguish the negative sequence current of the stator three-phase current caused by voltage imbalance or the fault alone in reference [17]. Reference [18], [19] observed both currents of the stator and rotor sides under normal and different interturn short-circuit faults, and the negative sequence current, Park's vector trajectory, and phase angle are discussed in all conditions. Motor Current Signal Analysis (MCSA) was chosen as the fault diagnosis method in reference [20]. The presented studies scientifically and effectively reflect the advantages of using the current signal in the interturn short-circuit fault detection, but they did not consider the effect of the position of the short-circuit slot on interturn short-circuit fault detection.

Recent studies have examined the effects of stator and rotor interturn short-circuit positions on diagnostic characteristics. Recently, an integrated formula for the cage-rotor induction machine interturn short-circuit fault detection considering the saturation effect has been presented [21]. Reference [22] further studied stator winding interturn short-circuit detection in induction motors by parameter identification. The air-gap flux density differences of the rotor interturn short-circuit faults in different positions of the generator have been performed by Li and Han [23]. The presented research results are more important complements to the analysis of the influence of the stator short-circuit position on the turbo-generator than on the DFIG.

In this paper, we consider both the different numbers of the fault turns and different fault positions. Based on the fault slots' location with respect to the quadrature-axis, the field-circuit coupling method is properly used for modeling the healthy or fault conditions of the generator. Improved DFIG models at different conditions of the stator winding interturn short-circuit fault are built in Maxwell 2D. The different settings of the excitation source on the stator winding, the phase winding connection, the values of end leakage inductance and resistance constitute different working conditions. The source and the harm of negative sequence current are explored for the necessity, and the MATLAB platform is used instead of the approximate calculation method to improve the accuracy of the calculated negative sequence current. The simulation results of different levels of stator winding interturn faults obtained by the FEM method with the ANSYS Maxwell are compared. Lastly, the complete comparisons of the time domain of the stator current and negative sequence current of the interturn faults in different slots show the influence of the short-circuit position and the effectiveness of the proposed technique.

The rest of this paper is organized as follows: section II briefly introduces the analysis of the negative sequence current of DFIG suitable for detecting stator interturn faults, and section III describes the modeling of DFIG based on the FEM basic theory. In addition, section IV introduces the simulation process of the stator winding interturn short circuit (SWITSC) fault in DFIG, amplitude analysis of the stator current, negative sequence current, and phase difference analysis of the stator current. Lastly, section V presents the conclusions.

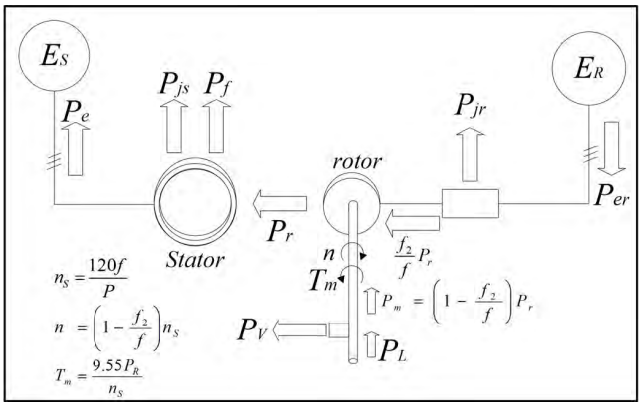

FIGURE 1. Power-flow plan of a DFIG operating at the sub-synchronous state.

II. ANALYSIS OF NEGATIVE SEQUENCE CURRENT OF DFIG SUITABLE FOR DETECTING STATOR INTERTURN FAULTS

Power flow in a typical DFIG operating at sub-synchronous speed is shown in Figure 1. In the super-synchronous state, the power flow via the rotor loop is reversed so the electrical power can also be transmitted to the grid through the rotor.

In Figure 1, P is pole number; f is the output frequency of the stator side, f_2 is the rotor current frequency; n is the rotor's own speed, n_s is the synchronous speed, P_m is the mechanical power, P_r is the electromagnetic power of stator side, P_e is the electromagnetic power transmitted to the grid, P_{er} is the electromagnetic power transmitted by the power grid to the rotor through the converter, and T_m is the electromagnetic torque.

A. NEGATIVE SEQUENCE CURRENT MAPPED TO THE SHORTED POSITION OF THE SWITSC FAULT

After the stator winding interturn short-circuit fault occurs, the generator operates in the asymmetrical state and the negative sequence current component will generate in the stator windings. The short-circuit current can be regarded as a superposition of the normal current and the current in the same direction as the original current. By assuming i_g is the current flowing through a single-turn coil of stator windings of the DFIG, the magnetomotive force (MMF) of the single-turn coil can be regarded as the synthesis of two conductors' MMF. The currents of the two conductors are equal in magnitude and opposite in direction. The Fourier expansion formula of the MMF of the single-turn coil concluded by

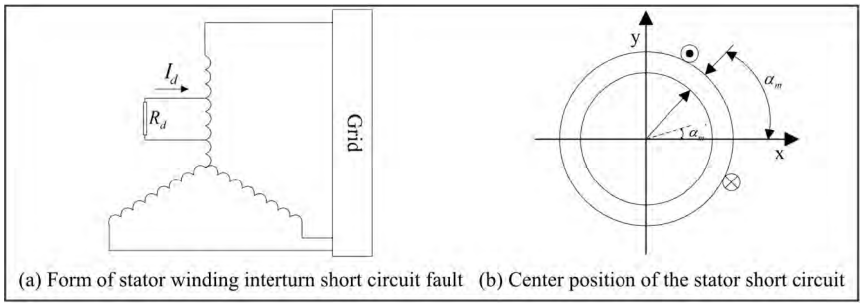

(a) Form of stator winding interturn short circuit fault (b) Center position of the stator short circuit

FIGURE 2. Diagrams of stator interturn fault.

strict derivation is written as

$$F(\alpha) = \frac{2i_g}{\pi P}\sum_{\upsilon}\frac{1}{\upsilon}k_{yf}\cos(\upsilon\alpha) \tag{1}$$

where $k_{yf} = \sin\left(\upsilon\alpha_y/2\right)$ is the coil pitch factor and α_y is the space electrical angle between two conductors; $\upsilon = 1/P, 2/P, 3/P, \ldots$ is for the short pitch coil, but $\upsilon = 1/P, 2/P, 3/P, \ldots \& \upsilon \neq 2, 4, 6, \ldots$ is for the full-pitch winding.

When the stator winding interturn short-circuit fault occurs in a generator, it is assumed that a current in the same direction as the original current is superimposed on the short-circuit turn, and the magnetic field created in the air gap by the current is superimposed with the magnetic field of the generator under normal condition; in other words, the synthetic air-gap magnetic field of the generator with the stator winding interturn short-circuit fault [24].

We assume $i_f = \sqrt{2}\,I\cos(\omega t)$ is superimposed on the short-circuit turn. According to equation (1), the MMF can be expressed as follows:

$$\begin{aligned} F(\alpha, t) &= \frac{2\sqrt{2}I}{\pi P}\sum_{\upsilon}\frac{1}{\upsilon}k_{yf}\cos(\omega t)\cos(\upsilon\alpha) \\ &= \frac{\sqrt{2}I}{\pi P}\sum_{\upsilon}\frac{1}{\upsilon}k_{yf}\cos(\omega t \pm \upsilon\alpha) \end{aligned} \tag{2}$$

where $\omega = 2\pi f$ is the angular frequency of the power supply.

Equation (2) shows that the MMF of the current i_f superimposed on the short-circuit turn is a pulsating MMF, which can be decomposed into two circular rotating magnetomotive forces with the same amplitude and rotational speed but turning in the opposite direction. The reverse-rotating circular magnetomotive force induces a negative sequence current. The stator negative sequence current can be selected as one of the characteristic quantities of the stator winding interturn short-circuit fault of the generator, which can effectively diagnose stator faults of the generator based on the theory.

The unit area air-gap permeance is the constant not affected by the stator winding interturn short-circuit fault of the generator according to the stator winding interturn short-circuit fault form, as shown in Figure 2(a). The radial air-gap length of the generator is g and the air-gap circum-ferential angle is α_m. After ignoring the higher harmonics, the pulsating magnetic potential is

$$\begin{aligned} f_d(\alpha_m, t) &= F_d\cos\omega t\cos(\alpha_m - \alpha'_m) \\ &= F_{d+}\cos\left(\omega t + \alpha_m - \alpha'_m\right) \\ &\quad + F_{d-}\cos\left(\omega t - \alpha_m + \alpha'_m\right) \end{aligned} \tag{3}$$

where α'_m is the mechanical angle of the center position of the stator short circuit, as shown in Figure 2(b). The first item in the formula $F_{d+} = F_{d-} = F_d/2$ is the magnetic potential that rotates in the same direction as the rotor and induces the positive sequence current in the three-phase winding of the stator. The second item is the magnetic field that rotates in the opposite direction with the rotor and induces negative sequence current in the three-phase winding of the stator. While the short-circuit fault occurs in the different short-circuit slots, the air-gap circum-ferential angle α_m is the same, but the mechanical angle of the center of the short-circuited stator is different, and α'_m of fault in the slot 19# is greater than that in slot 4#. Thus, the components of induced positive and negative sequence currents in different fault conditions exist. Based on this difference, it can be further supplemented as a basis for stator winding interturn fault diagnosis.

B. CALCULATION METHOD OF NEGATIVE SEQUENCE CURRENT

Accurately measuring and calculating the negative sequence current are needed to detecting the abnormal operating state of the generator, ensuring the safe and reliable operation of the system, and correctly setting the relay protection device.

We assume that asymmetrical currents are $\dot{I}_A, \dot{I}_B, \dot{I}_C$, and these can be decomposed into positive sequence current, negative sequence current, and zero-sequence current according to the symmetrical components method shown in equation (4).

$$\left.\begin{aligned} \dot{I}_1 &= \tfrac{1}{3}\left(\dot{I}_A + a\dot{I}_B + a^2\dot{I}_C\right) \\ \dot{I}_2 &= \tfrac{1}{3}\left(\dot{I}_A + a^2\dot{I}_B + a\dot{I}_C\right) \\ \dot{I}_0 &= \tfrac{1}{3}\left(\dot{I}_A + \dot{I}_B + \dot{I}_C\right) \end{aligned}\right\} \tag{4}$$

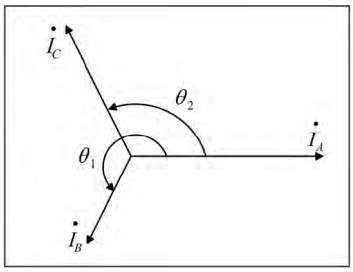

FIGURE 3. Phasor diagram of asymmetrical currents.

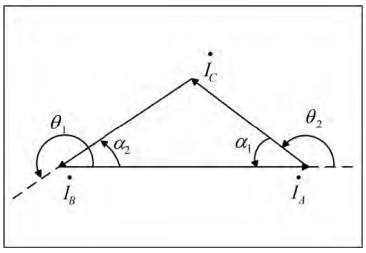

FIGURE 4. Closed triangle formed by $\dot{I}_A, \dot{I}_B, \dot{I}_C$.

where $a = 1\angle 120° = e^{j120°} = -(1/2) + j\sqrt{3}/2$.

Each sequence current can be calculated according to equation (4) when $\dot{I}_A, \dot{I}_B, \dot{I}_C$ are known. However, the effective values of the three-phase currents are known normally. Thus, equation (4) cannot be applied directly, and the initial phase angle of each phase current must be obtained first. The asymmetrical currents are shown in Figure 3, where $\dot{I}_A = \underset{A}{I}\, e^{j0°}, \dot{I}_B = \underset{B}{I}\, e^{j\theta_1}, \dot{I}_C = \underset{C}{I}\, e^{j\theta_2}$.

The phasor sum of the three currents is a closed triangle, as shown in Figure 4. The initial phase angles θ_1 & θ_2 to the currents of B-phase and C-phase are shown in Figure 4.

According to cosine theorem, these angles can be obtained as follows:

$$\left.\begin{aligned} \cos\theta_1 &= \cos(180° + \alpha_2) = \frac{I_A^2 + I_B^2 - I_C^2}{2I_A I_B} \\ \cos\theta_2 &= \cos(180° - \alpha_1) = \frac{I_A^2 + I_C^2 - I_B^2}{2I_A I_C} \end{aligned}\right\} \quad (5)$$

Negative sequence current I_2 in the absence of zero-sequence current can be worked out according to equations (4) and (5), but the complex operation is involved in Equation (4), resulting in a tedious calculation process.

To improve the calculation accuracy of the negative sequence current, MATLAB is used to directly program equations (4) and (5). After the execution, as long as the three-phase current I_A, I_B, I_C are inputted according to the prompt, the negative sequence and positive sequence currents can be calculated individually, and the phasor diagrams of positive sequence, negative sequence, and three-phase current can be drawn at the same time.

III. MATHEMATICAL MODELING OF THE MODIFIED SWITSC FAULT

A. TWO-DIMENSIONAL DISCRETIZATION AND PIECEWISE INTERPOLATION

The finite element method calculates the numerical solution of a system based on the boundary condition and one specific initial condition.

The generator is equivalent to an inductance element, and the magnetic field as a medium makes the generator realize the conversion of electromechanical energy [25]. After Maxwell's creative equation of the electromagnetic field was developed, a new theoretical basis for the study and analysis of the electromagnetic field in the generator was provided.

The entire circumferential surface of the axial cross section of the generator is the considered calculation region. Because the current source exists in the calculation region, the magnetic vector potential is used to calculate the solution. With the axial components of the magnetic vector potential A_Z being expressed, the expression of the boundary value problem of DFIG in the magnetic field is

$$\begin{cases} \dfrac{\partial}{\partial x}\left(\dfrac{1}{\mu}\dfrac{\partial A_Z}{\partial x}\right) + \dfrac{\partial}{\partial y}\left(\dfrac{1}{\mu}\dfrac{\partial A_Z}{\partial y}\right) = -J_Z \\ A_Z|_{\overline{AB},\overline{CD}} = 0 \\ A_Z|_{\overline{AD}} = -A_Z|_{\overline{BC}} \end{cases} \quad (6)$$

In equation(6), J_Z is the z component of the source current density, and μ is the permeability of the material.

The above equation is equivalent to the following expression of the variational problem

$$\begin{cases} W(A_Z) = \iint \left\{ \dfrac{1}{2 \bullet \mu}\left[\left(\dfrac{\partial A_Z}{\partial x}\right)^2 + \left(\dfrac{\partial A_Z}{\partial y}\right)^2\right] - A_Z J_Z \right\} \\ \qquad dxdy = \min \\ A_Z|_{\Gamma_1\Gamma_2} = 0 \end{cases} \quad (7)$$

where 0 is the given value of A_Z on the boundary of Γ_1 and Γ_2. The two-dimensional finite element method starts with equation (7), and the solution region is separated and dispersed. The interpolation function of the magnetic vector potential is constructed in the discrete element and then the conditional variation problem in equation (7) is discretized into the extreme value problem of the multivariate function by the difference method.

B. GEOMETRICAL POSITIONS AND WINDING MODELING

This research simulates a 0.55 kW wound rotor three-phase double-fed induction generator, and the specific parameters and the required type of this DFIG are listed in Table I.

In this paper, each phase of the stator winding has only one branch, so the SWITSC fault belongs to the interturn short circuit in the same branch. Phase C is taken as an example, and Figure 5 and Figure 6 show the different geometrical models of the SWITSC fault, which one model is at slot

TABLE 1. Parameters of the simulated DFIG.

Parameter	Value(Stator/Rotor)
Number of poles	4/4
Number of slots	30/24
Circuit type	Y/Y
Outer Diameter	180/120 mm
Inner Diameter	121/50 mm
Length	65 mm
Winding layers	2/2
Parallel branches	1/1
Rated power factor	0.95
Rated output power	0.55 kW
Rated speed	1500 r·min^{-1}
Rated voltage	220 V
Frequency	50 Hz
Frictional loss	12 W
Operating temperature	75 □

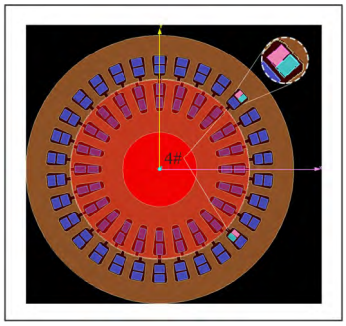

FIGURE 5. The model of the SWITSC fault at slot 4#.

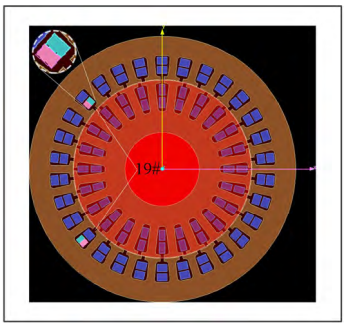

FIGURE 6. The model of the SWITSC fault at slot 19#.

4# and another model is at slot 19#. The fault is located in one slot of phase C, and the branch is divided into two parts: short-circuit winding and non-short-circuit winding. The slot corresponding to the fault slot is made the same geometrical change. Based on the field-circuit coupling method, the geometry, the distribution parameters, the saturation of the ferromagnetic material, and the eddy current effect of the motor are well considered, allowing insight into the electromagnetic, thermal, and stress states of the various points inside the motor [26]. To achieve these effects, the external circuit of the SWITSC fault is set and is shown in Figure 7.

IV. SIMULATION AND RESULTS DISCUSSION

A. THE SWITSC FAULT SIMULATION OF DFIG

The synchronous speed of the machine was 1500 r·min^{-1}. Different working conditions of the DFIG were all simulated

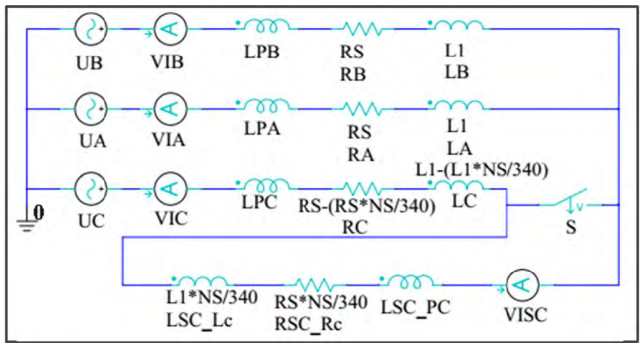

FIGURE 7. The external circuit of the SWITSC fault.

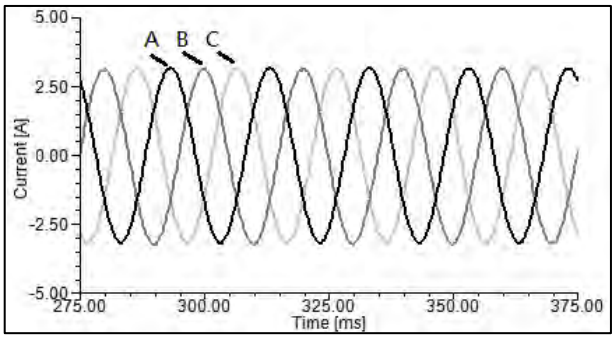

FIGURE 8. Stator current of DFIG on the healthy grid-connected operation.

in ANSYS Maxwell at the constant super-synchronous speed of 1660 r·min^{-1}. The grid frequency was set to 50 Hz, and −5.3 Hz was the frequency of the rotor side current according to the principle of VSCF of the DFIG [27]–[29].

The geometrical models and the external circuit of the SWITSC fault are shown in Figures 5, 6, and 7. The entire time for the simulation of the generator was 0.6 s, and the generator was operating on the grid-connected normal state before t = 0.3 s. At t = 0.3 s, the SWITSC fault was obtained by controlling the switch to close the short-circuit switch and form a new loop. Five fault levels and two different shorted slots are emulated, and the number of interturn short-circuit faults were 5, 10, 15, 20 and 25 turns. Because the total number of turns was 340, the respective percentages of interturn short-circuit fault were 1.5%, 2.9%, 4.4%, 5.9%, and 7.3%.

B. AMPLITUDE ANALYSIS OF STATOR CURRENT

Figure 8 gives the stator current of DFIG on the healthy grid-connected operation from 275 ms to 375 ms. The figure shows that the current simulation waveform of the three phases was symmetrical, the magnitude of the standard sinusoidal waveform was 3.1 A, and the phase difference of the currents was about 120°, further proving the correctness of establishing the two-dimensional electromagnetic field model of the doubly-fed generator in ANSYS Maxwell. Then, the failure state was examined. Figure 9 and Figure 10 show the stator current of DFIG on the SWITSC fault operation with two different short-circuit slot positions from 280 ms to 380 ms.

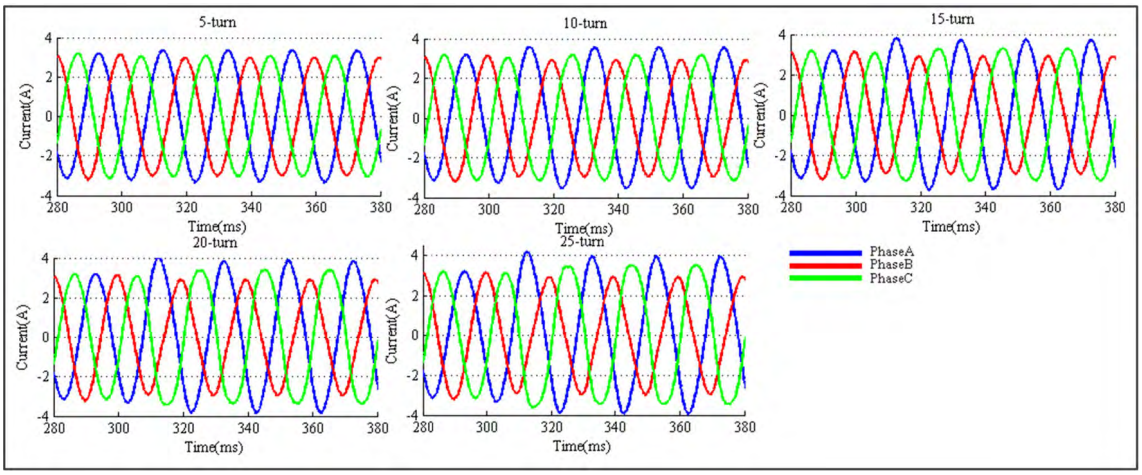

FIGURE 9. Stator current of the SWITSC fault in DFIG at slot 4# under different turns of the interturn fault.

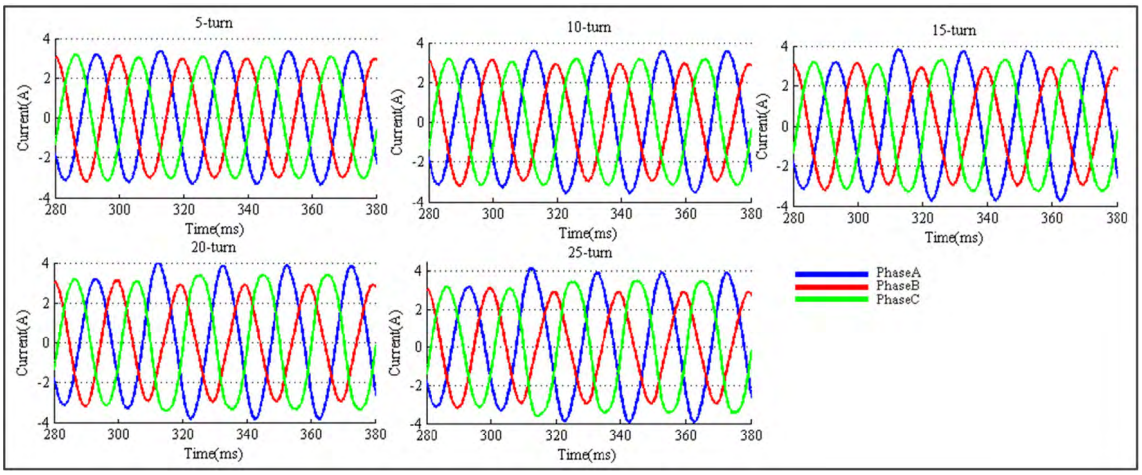

FIGURE 10. Stator current of the SWITSC fault in DFIG at slot 19# under different turns ot the interturn fault.

Figures 9 and 10 show that the overall trend of failure is the same. Before the failure, the waveform from 280 ms to 300 ms is uniform with the same amplitude of the three-phase current that stabilizes at 3.2 A, and the phase differences of current were about 120°. The currents changed at t = 0.3 s when the fault occurred. The minor fault with 5 turns short had a slight effect. As the degree of failure increases, the instantaneous value of the A-phase current during the 20 turns short-circuit condition increases to 4 A and stabilizes around 3.8 A, and the amplitudes of the B-phase current and the C-phase current change significantly. The abrupt change of the 25-turns short-circuit condition was larger than changes under the other conditions. Next, the current differences between Figures 9 and 10 because of the fault location were analyzed.

Because the C-phase was set to the fault phase, the change law of the phase was analyzed. Figure 11 shows the changes of the C-phase current for faults occurring at different levels of faults at slot 4 # and slot 19#. The figure shows that the short-circuit phase current increases with an increased number of short-circuit turns. The same change rule exists whether the fault occurs in slot 4#, which is close to the quadrature-axis, or slot 19#, which is far from the quadrature-axis.

The difference and effect of the current amplitude characteristics caused by the faults occurring in different slots were analyzed. The differences between Figure 9 and Figure 10 are showed in Figure 12 and were based on the data refinement results. Figure 12 shows that the currents of the non-short-circuit phases (A-phase & B-phase) affected by the interturn short-circuit fault located in the slot 4# were higher in the display range. When interturn short-circuit fault occurs, the distance relative to the quadrature-axis leads to different relative air-gap magnetic densities, thus resulting in different phase currents when short-circuit occurs in different slots. The negative sequence current produced by the short-circuit fault in the slot that is close to the quadrature-axis is less than that produced by the same fault in the slot that is far away from the quadrature-axis. This effect is embodied in the higher current of the non-short-circuit phase and the lower

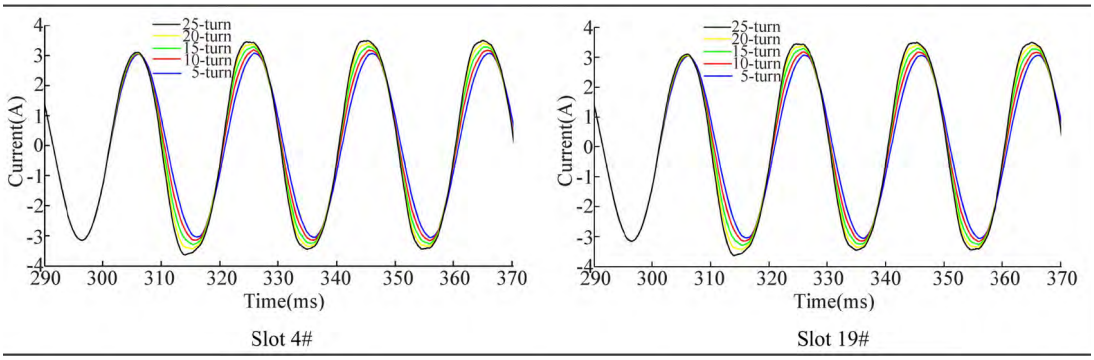

FIGURE 11. C-phase current of the SWITSC fault in DFIG at slot 4# and slot 19# under different turns of the interturn fault.

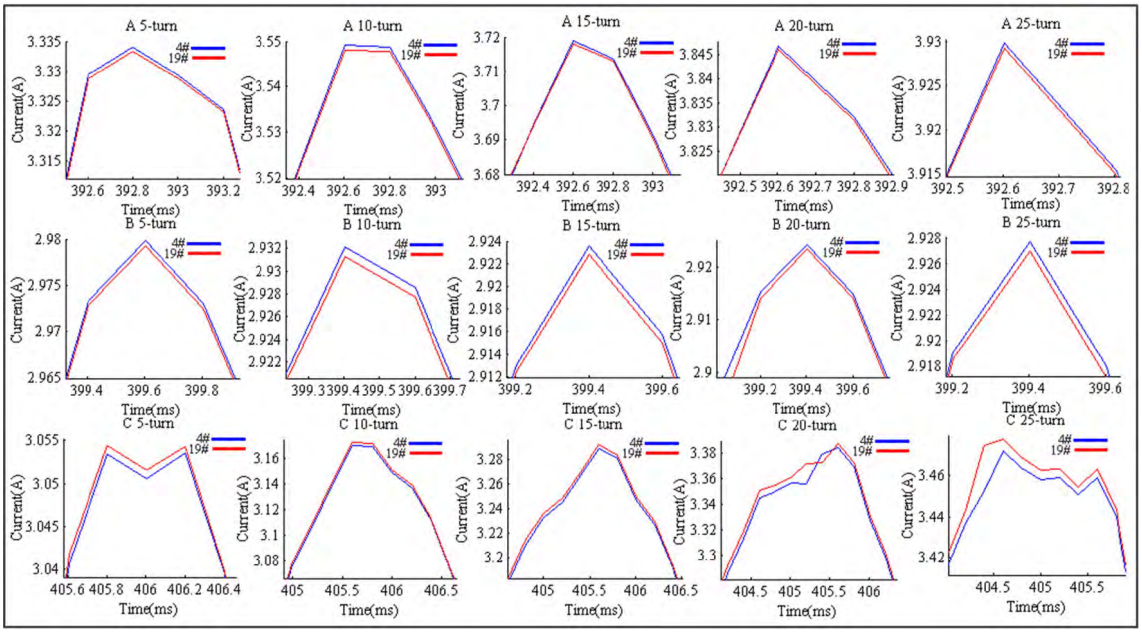

FIGURE 12. tator current comparison diagram between SWITSC fault at slot 4# and slot 19# in DFIG under different turns of the interturn fault.

current of the short-circuit phase. As the models were set, slot 4# was close to the quadrature-axis while slot 19# was far from the quadrature-axis. In addition, phase C was the fault phase. The current difference and absolute value of the current difference were obtained according to $I_{4\#} - I_{19\#}$ and $|I_{4\#} - I_{19\#}|$, which are shown in Figure 13(a) and (b), respectively. Overall, the current difference of non-fault phases under the influence of different fault positions does not change with the deepening of the fault level, although for the short-circuit fault of 5 and 10 turns, the data of A-phase are not in linear, but the outcome is not affected. The absolute value of the current difference of the fault phase has increased following the deepening of the failure, and it can be used as a diagnostic basis for stator winding turn shorts occurring in different slots of the stator.

To supplement the multi-speed working condition in this paper, the sub-synchronous state with a rotor speed at 1400r·min^{-1} was analyzed.

TABLE 2. Amplitudes of the three-phase currents under rotor speeds.

Speeds	I_A/A	I_B/A	I_C/A
1400r·min^{-1}	3.709	2.918	3.273
1660r·min^{-1}	3.742	2.919	3.276

When the fault was located at slot 4# and the turn number of interturn short-circuit fault are 15 turns, the stator currents of the generator under the rotor speed at 1400r·min^{-1} and 1660r·min^{-1} were compared, as shown in Figure 14, and the statistical amplitudes of the three-phase currents are filled in Table II.

Figure 12 and Table II show that the amplitude of each phase current under the super-synchronous state is larger than that under the sub-synchronous state, proving the generation efficiency of the super-synchronous state is higher than that of the sub-synchronous state, and that the current increases with

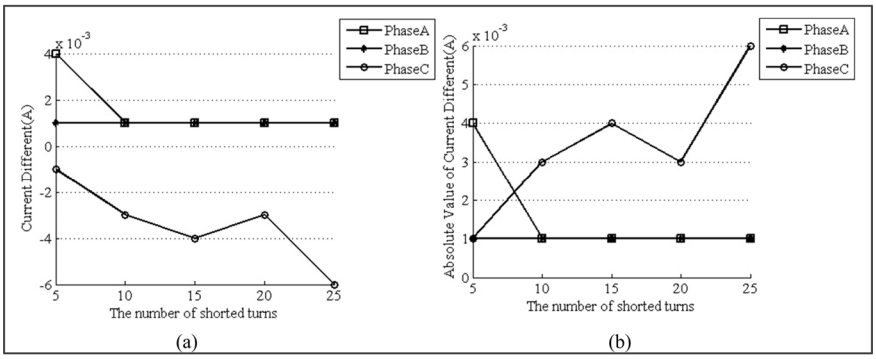

FIGURE 13. Current different and the absolute value of it between the SWITSC fault at slot 4# and slot 19# under different turns of the interturn fault.

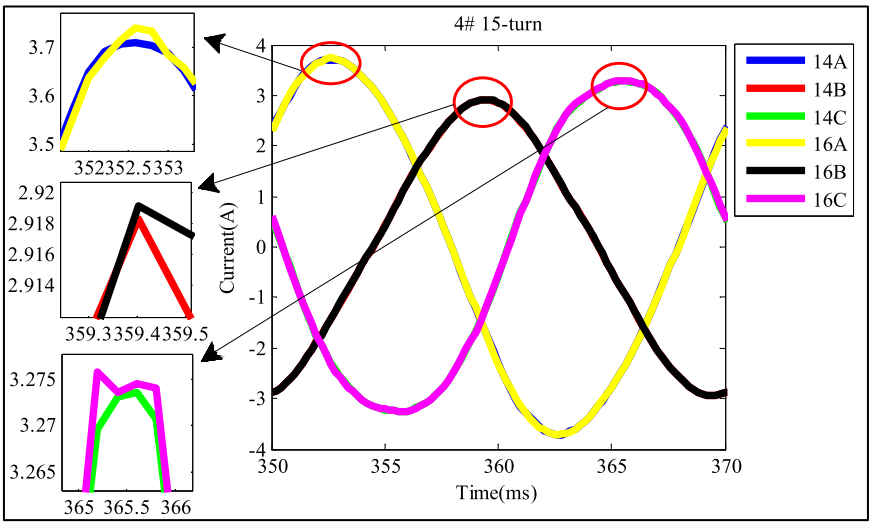

FIGURE 14. Stator currents under different rotor speeds.

increased rotating speed, which yielding the power relation and operation principle of DFIG.

Confirming the correctness of the model under the sub-synchronous state, the simulation models set with different short-circuit slots are compared in this paper. In this model, The rotor speed is 1400r·min^{-1} and the short-circuit turns is 15 turns.

Figure 15 shows the comparison diagram of the stator three-phase current waveform of the fault at two different slots, and it is compared with the local amplification current diagram of 15 short-circuit turns when the generator is at 1660r·min^{-1}. Besides, the amplitudes of the three-phase currents at 1400r·min^{-1} are presented in Table III.

Figure 15 shows that when the generator is in the sub-synchronous state with a rotation speed of 1400r·min^{-1}, the amplitudes of phase A and phase B currents when the short-circuit fault occurs in slot 4# were higher than that when the short circuit occurs in slot 19#. The amplitude of C-phase current when the short-circuit fault occurred in slot 19# was higher than that when the short-circuit position was in slot 4#. This conclusion is the same as when in the super-synchronous state with a rotation speed of 1660r·min^{-1}. Therefore, the above comparison shows that the method of judging different short-circuit slots proposed in this paper is applicable to different rotating speed conditions.

TABLE 3. Amplitudes of the three-phase currents under 1400r·min^{-1} rotor speed.

Slots	I_A/A	I_B/A	I_C/A
4#	3.709	2.933	3.264
19#	3.707	2.932	3.266

C. NEGATIVE SEQUENCE CURRENT AND PHASE DIFFERENCE ANALYSIS OF STATOR CURRENT

In this section, the negative sequence current I_2 and the positive sequence current I_1 under the five interturn short-circuit fault conditions in two different fault slots were calculated based on the MATLAB, and the complete comparison and values for the different fault levels are presented in Table IV. The ratios of I_2 and I_1 were also obtained and are shown in

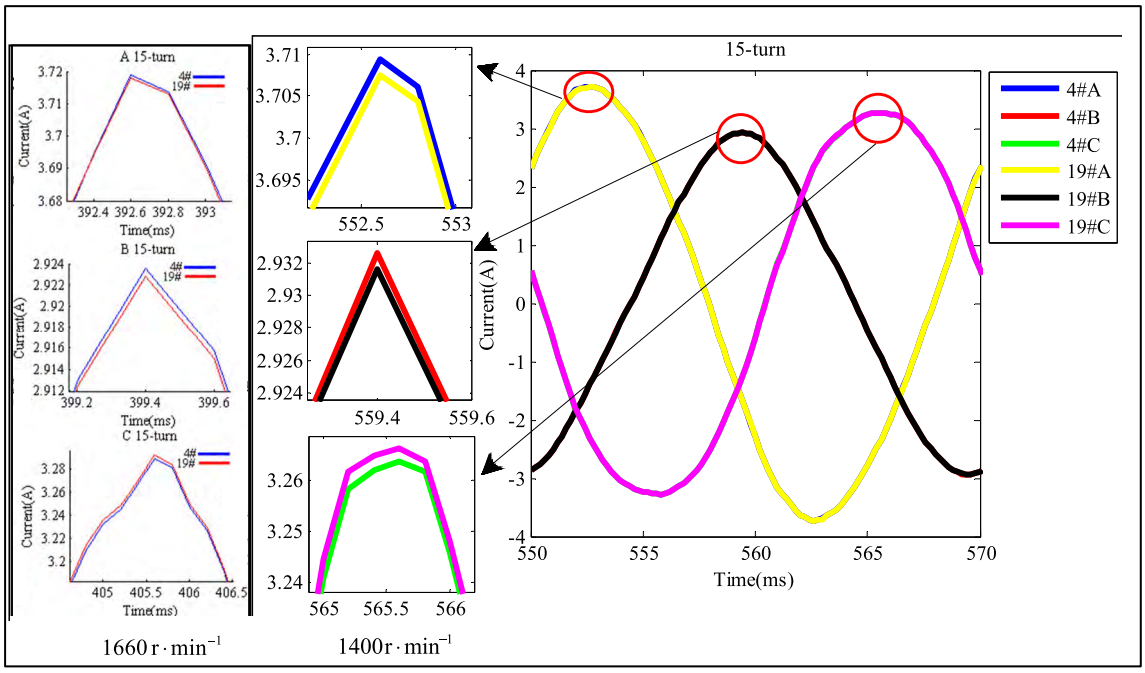

FIGURE 15. Stator currents of the SWITSC fault at slot 4# and slot 19# under different rotor speed.

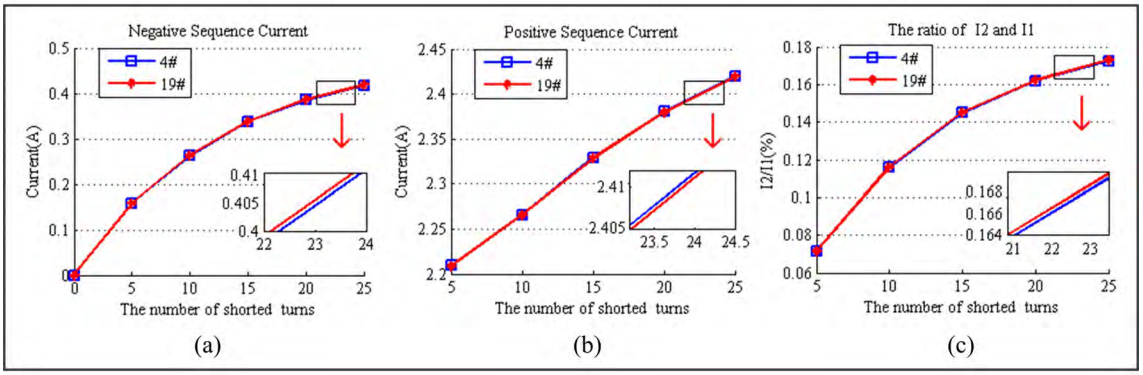

FIGURE 16. The line charts of negative sequence current, positive sequence current, and the ratio for stator winding faults under different conditions.

this table. According to this table, Figure 16(a), (b), and (c) are plotted.

Figure 16(a) shows that when interturn short-circuit fault occurs, the value increases with the number of shorted turns. The enlarged part in the figure shows that when the fault occurs in the slot 19# of the stator, the negative sequence current content is more than that effected by the fault occurring in the slot 4#. This is similar to the current amplitude comparison of the fault phase (C-phase) in the Figure 12 of part B. Figure 16(c) is similar to the shape and trend of the curve in Figure 16(a), means the ratio of the negative sequence current to the positive sequence current increases with the degree of failure.

Similarly, Figure 16(b) shows that the positive sequence current increases as the fault level deepens, but the amplification section shows that positive sequence current content affected by the fault occurred in slot 19#, which is far from the quadrature-axis, was lower and similar to the comparison of the current amplitude of the non-failure phases (A-phase and B-phase) in the Figure 12 of part B.

After analyzing the negative sequence component, the phase differences for the commonality and heterogeneity of the phase differences were analyzed when the interturn short-circuit faults were in different slots in the super-synchronous state. The phase differences for stator winding faults under different conditions of this DFIG are presented in Table V.

Table V shows that when C-phase occurs, the interturn short circuit and the phase angles of current are no longer 120°. The phase difference between A-phase and B-phase

TABLE 4. Negative and positive sequence currents and ratios for stator winding faults under different conditions.

The number of shorted turns	I_2 /A		I_1 /A		I_2 / I_1 /%	
	Slot 4#	Slot 19#	Slot 4#	Slot 19#	Slot 4#	Slot 19#
5	0.1579	0.1581	2.2092	2.2089	0.0715	0.0716
10	0.2622	0.2632	2.2660	2.2655	0.1157	0.1162
15	0.3372	0.3379	2.3287	2.3285	0.1448	0.1451
20	0.3851	0.3860	2.3802	2.3796	0.1618	0.1622
25	0.4175	0.4185	2.4196	2.4190	0.1725	0.1730

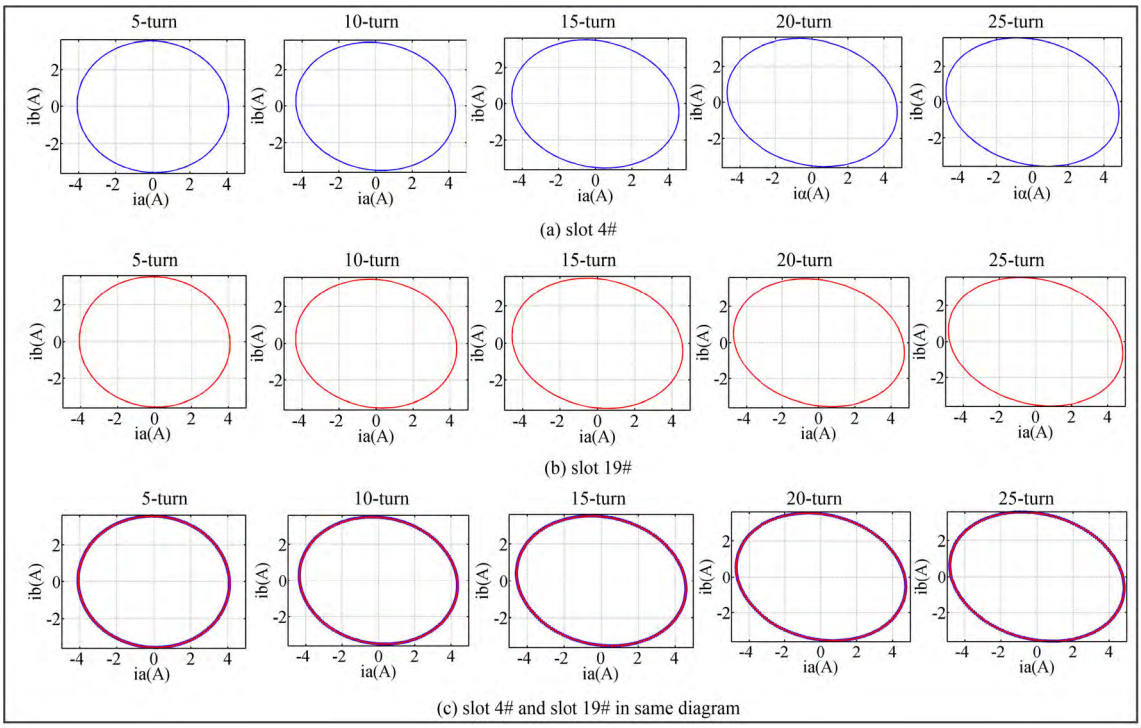

FIGURE 17. Park's vector trajectory for stator winding faults under different conditions.

TABLE 5. Phase difference for stator winding faults under different conditions.

The number of shorted turns	Phase difference (°)					
	AB		BC		CA	
	Slot 4#	Slot 19#	Slot 4#	Slot 19#	Slot 4#	Slot 19#
5	122.5629	122.5837	112.7906	112.7777	124.6465	124.6386
10	122.6908	122.7383	108.6726	108.6079	128.6366	128.6538
15	122.4420	122.4964	106.2196	106.1656	131.3384	131.3380
20	121.9894	122.0386	105.0190	104.9521	132.9916	133.0093
25	121.4818	121.5313	104.4278	104.3609	134.0904	134.1078

was greater than 120°, while the value decreases as the number of short-circuit turns increases. The phase difference of the fault-phase C and its lagging phase is more than 120°, but this phase difference was different from the previous non-failure phases and increased even to 134°.

All the angles of these two kinds of phases affected by the fault in the slot 4# were smaller. The opposite result of the phase difference occurs between the C-phase and its leading phase in which the value decreases to 104°. The stator short-circuit faults in the stator damage the symmetry of the phase difference, and the degree of damage is related to the degree of failure.

The Park's vector trajectory is a circle centered at the origin under normal conditions where the stator short-circuit faults make it be an ellipse. Figure 17 (a) and (b) display the Park's vector trajectories under five conditions in slot 4# and slot 19#, respectively. Figure 17 (a) and (b) both show the ellipse becomes flatter as the failure degree increases. To determine

TABLE 6. Park's vector trajectory for stator winding faults under different conditions.

The number of shorted turns	Length of the semi-major axis		Length of the semi-minor axis		Eccentricity	
	Slot 4#	Slot 19#	Slot 4#	Slot 19#	Slot 4#	Slot 19#
5	4.0971	4.0970	3.5603	3.5593	0.4948	0.4952
10	4.3637	4.3646	3.5239	3.5210	0.5898	0.5909
15	4.5917	4.5925	3.5565	3.5535	0.6325	0.6335
20	4.7546	4.7555	3.6212	3.6183	0.6480	0.6489
25	4.8707	4.8725	3.6956	3.6927	0.6514	0.6524

the differences of the Park's vector trajectories between the faults in slot 4# and slot 19#, the two trajectories are presented in one diagram (c), and Table VI shows the effective fault signatures including the lengths of semi-major axes, the lengths of the semi-minor axes, and the eccentricities of the ellipses. Eccentricity shows the distortion of the fault degree, and it was larger for the failure in slot 19#.

V. CONCLUSIONS

The finite element model of DFIG was built for simulations of different conditions. The amplitude, negative sequence current, and phase difference analysis of the stator current were explored when DFIG was in different SWITSC fault states. With the occurrence of the stator winding interturn short-circuit fault, the stator current was no longer stable. The results show that the negative sequence current under the influence of different short-circuit slots corresponds to the fault phase's current magnitude comparison and the positive sequence current corresponds to the non-fault phase's magnitude comparison. The fault slot that is either close to the quadrature-axis or far from the quadrature-axis has different effects on the phase difference. The proposed research methods and analytical methods in this paper provide the theoretical proof and the basis to the research on the positioning of DFIG with the stator winding interturn short circuit fault. However, only minority numbers of fault slots in the SWITSC fault are discussed and simulated, which cannot include all cases of interturn short circuit fault. Different numbers of shorted turns in different slot positions should be analyzed in the future.

ACKNOWLEDGMENT

The authors would like to thank the anonymous reviewers for their very valuable comments.

REFERENCES

[1] M. Malekpour, B. T. Phung, and E. Ambikairajah, "Modelling and diagnostic of incipient stator inter-turn short circuit fault in induction motors," in *Proc. Condition Monit. Diagnosis (CMD)*, Perth, WA, Australia, Sep. 2018, pp. 1–6.

[2] I. Tsyokhla, A. Griffo, and J. Wang, "Online condition monitoring for diagnosis and prognosis of insulation degradation of inverter-fed machines," *IEEE Trans. Ind. Electron.*, vol. 66, no. 10, pp. 8126–8135, Oct. 2019.

[3] S. Moon, H. Jeong, H. Lee, and S. W. Kim, "Interturn short fault diagnosis in a PMSM by voltage and current residual analysis with the faulty winding model," *IEEE Trans. Energy Convers.*, vol. 33, no. 1, pp. 190–198, Mar. 2018.

[4] J. A. Haylock, B. C. Mecrow, A. G. Jack, and D. J. Atkinson, "Operation of fault tolerant machines with winding failures," *IEEE Trans. Energy Convers.*, vol. 14, no. 4, pp. 1490–1495, Dec. 1999.

[5] R. Roshanfekr and A. Jalilian, "Analysis of rotor and stator winding inter-turn faults in WRIM using simulated MEC model and experimental results," *Electr. Power Syst. Res.*, vol. 119, pp. 418–424, Feb. 2015.

[6] R. Roshanfekr and A. Jalilian, "Wavelet-based index to discriminate between minor inter-turn short-circuit and resistive asymmetrical faults in stator windings of doubly fed induction generators: A simulation study," *IET Gener., Transmiss. Distrib.*, vol. 10, no. 2, pp. 374–381, Feb. 2016.

[7] M. K. Dösoğlu and A. B. Arsoy, "Transient modeling and analysis of a DFIG based wind farm with supercapacitor energy storage," *Int. J. Electr. Power Energy Syst.*, vol. 78, pp. 414–421, Jun. 2016.

[8] O. Jinxin, D. Yanbo, Z. Di, Y. Rui, Z. Xi, and X. Xiaofu, "Dynamic equivalent model of doubly fed wind farm during electromagnetic transient process," *IET Renew. Power Gener.*, vol. 11, no. 1, pp. 100–106, Nov. 2017.

[9] Z. Xu, C. Hu, F. Yang, S.-H. Kuo, C.-K. Goh, A. Gupta, and S. Nadarajan, "Data-driven inter-turn short circuit fault detection in induction machines," *IEEE Access*, vol. 5, no. 1, pp. 25055–25068, 2017.

[10] A. Yazidi, H. Henao, G. A. Capolino, L. Capocchi, and D. Federici, "Double-fed three-phase induction machine model for simulation of inter-turn short circuit fault," in *Proc. IEEE Int. Electr. Mach. Drives Conf.*, Miami, FL, USA, May 2009, pp. 571–576.

[11] B. Dosijanoski, Simulation of doubly-fed induction generator in a wind turbine, in *Proc. 11th Int. PhD Workshop*, Oct. 2009, pp. 17–20.

[12] L. Jun-Qing and W. Xi-Mei, "FEM analysis on interturn fault of rotor wingding in DFIG," in *Proc. Int. Conf. Elect. Mach. Syst. (ICEMS)*, Busan, South Korea, Oct. 2013, pp. 797–802.

[13] Y. Chen, L. Wang, Z. Wang, A. U. Rehman, Y. Cheng, Y. Zhao, and T. Tanaka, "FEM simulation and analysis on stator winding inter-turn fault in DFIG," in *Proc. 11th IEEE Int. Conf. Properties Appl. Dielectric Mater. (ICPADM)*, Sydney, NSW, Australia, Jul. 2015, pp. 244–247.

[14] L. Un-Qing, M. Li, and W. De-yan, "Influence of stator turn-to-turn short-circuit on magnetic field of DFIG," in *Proc. Int. Conf. Elect. Mach. Syst.*, Beijing, China, Aug. 2011, pp. 1–5.

[15] M. Y. Kia, M. Khedri, H. R. Najafi, and M. A. S. Nejad, "Hybrid modelling of doubly fed induction generators with inter-turn stator fault and its detection method using wavelet analysis," *IET Gener., Transmiss. Distrib.*, vol. 7, no. 9, pp. 982–990, Sep. 2013.

[16] A. U. Rehman, Y. Chen, L. Wang, Y. Zhao, Y. Cheng, and T. Tanaka, "Simulation using MATLAB/Simulink on rotor winding inter-turn short circuit fault in DFIG," in *Proc. IEEE Int. Conf. Dielectr. (ICD)*, Montpellier, France, Jul. 2016, pp. 506–509.

[17] J. Li, W. Kang, and L. Shen, "Simulation research on stator winding inter turn short circuit fault of doubly fed induction generator based on negative sequence current method under unbalanced voltage," *Electr. Mach. Control Appl.*, vol. 43, no. 11, pp. 80–85, Nov. 2016.

[18] Y. Zhao, Y. Chen, L. Wang, A. U. Rehman, Y. Cheng, Y. Zhao, B. Han, and T. Tanaka, "Experimental research and feature extraction on stator inter-turn short circuit fault in DFIG," in *Proc. IEEE Int. Conf. Dielectr. (ICD)*, Montpellier, France, Jul. 2016, pp. 510–513.

[19] Y. Zhao, Y. Chen, L. Wang, A. U. Rehman, Y. Yin, Y. Cheng, and T. Tanaka, "Experiment research and analysis of stator winding short circuit faults in DFIG," in *Proc. Int. Conf. Condition Monit. Diagnosis (CMD)*, Xi'an, China, Sep. 2016, pp. 160–163.

[20] J. Li, H. Yu, and L. Zhang, "Application of ensemble empirical mode decomposition on stator inter-turn short-circuit fault in doubly fed induction generators," in *Proc. 2nd Int. Conf. Mechatronics Autom. Control*, in Lecture Notes in Electrical Engineering, vol. 334. Cham, Switzerland: Springer, 2015, pp. 73–83.
[21] P. Naderi, "Inter-turn short-circuit fault detection in saturable squirrel-cage induction motor using magnetic equivalent circuit model," *Int. J. Comput. Math. Elect. Electron. Eng.*, vol. 35, no. 1, pp. 245–269, 2016.
[22] H. Abdallah and K. Benatman, "Stator winding inter-turn short-circuit detection in induction motors by parameter identification," *IET Electr. Power Appl.*, vol. 11, no. 2, pp. 272–288, Feb. 2017.
[23] Y. Li and B. Han, "Magnetic field finite element analysis of generator with rotor inter-turn short-circuit fault," *Appl. Mech. Mater.*, vol. 707, pp. 343–347, Dec. 2014.
[24] S.-M. M. Moosavi, J. Faiz, M. B. Abadi, and S. M. A. Cruz, "Comparison of rotor electrical fault indices owing to inter-turn short circuit and unbalanced resistance in doubly-fed induction generator," *IET Electr. Power Appl.*, vol. 13, no. 2, pp. 235–242, Feb. 2019.
[25] Q. Han, J. Wang, and Q. Li, "Finite element analysis of stiffness characteristics of an electromagnetic device," *J. Vib. Control*, vol. 18, no. 1, pp. 141–160, Jun. 2012.
[26] T. A. Nyamusa and N. A. Demerdash, "Transient analysis of partial armature short-circuit in an electronically commutated permanent magnet motor systen using an integrated nonlinear magnetic field-network model," *IEEE Trans. Energy Convers.*, vol. EC-2, no. 1, pp. 86–92, Mar. 1987.
[27] A. Soundarrajan, S. Sumathi, and G. Sivamurugan, "Voltage and frequency control in power generating system using hybrid evolutionary algorithms," *J. Vib. Control*, vol. 18, no. 2, pp. 214–227, Aug. 2012.
[28] Y. Ren, L. Cao, J. Zhou, L. Liu, M. Zhang, and H. Li, "The modeling and control of VSCF DFIG wind power generation based on PSCAD," in *Proc. Int. Conf. Intell. Control Inf. Process.*, Aug. 2010, pp. 24–28.
[29] M. Liu, W. Pan, R. Quan, H. Li, T. Liu, and G. Yang, "A short-circuit calculation method for DFIG-based wind farms," *IEEE Access*, vol. 6, pp. 52793–52800, 2018.

SHUILONG HE received the B.E. and M.E. degrees from Guangxi University, in 2010, and the Ph.D. degree from Xi'an Jiaotong University, in 2014.

He engages in the joint Postdoctoral work with Dongfeng Liuzhou Motor Company Ltd. and Xi'an Jiaotong University. He is currently an Associate Professor of mechanical engineering with the Guilin University of Electronic Technology. He has long been engaged in the application and research of dynamic system modeling, fault diagnosis, signal processing, and structural health monitoring. He presides over one major project of innovation-driven in Guangxi, one science and technology development project in Liuzhou, and one Guangxi Key Laboratory project. He participated in and completed three National Natural Science Foundations of China and one project of the Guangxi Innovation Team. He has applied for more than 20 invention patents and has published more than 20 papers in domestic and foreign journals, including more than ten papers retrieved by SCI/EI.

XUHONG SHEN received the B.E. degree in mechanical engineering from Huzhou University, in 2016. She is currently pursuing the master's degree in engineering with the Guilin University of Electronic Technology.

Her research interests include the application and research of dynamic system modeling, fault diagnosis, signal processing, and structural health monitoring. She participates in one Guangxi Key Laboratory project.

ZHANSI JIANG received the Ph.D. degree in mechanical engineering, in 2008.

He engaged in Postdoctoral research with Guilin Machine Tool Company Ltd., from 2010 to 2014, and engaged in Postdoctoral research with the Product Design Optimization Laboratory, Simon Fraser University, Canada, from 2012 to 2013. He is currently a Professor of mechanical engineering with the Guilin University of Electronic Technology. He presided over and completed one National Natural Science Foundation Project of China and one Postdoctoral Science Foundation Project of China. He presides over one National Natural Science Foundation Project of China and one Guangxi Key Laboratory of Manufacturing System and Advanced Manufacturing Technology Project. He has authored more than 24 academic papers, including more than 16 papers retrieved by SCI/EI and holds more than 14 inventions.

Dr. Jiang is a member of the Rotor Dynamics Branch of the Vibration Engineering Society of China. He received one Second Prize of the Natural Science Award of the National Department of Education. He serves as a Reviewer of *Shock and Vibration*, the *Journal of Vibroengineering*, and the *Journal of Applied Mechanics*.